communications earth & environment

Article

A Nature Portfolio journal

https://doi.org/10.1038/s43247-025-02453-4

Foliar methane and nitrous oxide fluxes in *Salix bebbiana* respond to light and soil factors

Md Rezaul Karim ✉, Md Abdul Halim & Sean C. Thomas

Foliar exchange of methane and nitrous oxide is a significant yet poorly understood component of global greenhouse gas budgets. To address this knowledge gap, we investigated foliar methane and nitrous oxide fluxes in *Salix bebbiana*, under varying light conditions (0–2000 μmol·m^{-2}·s^{-1}), soil aeration, and nitrogen availability, manipulated via biochar incorporation and nitrogen additions. Using rapid spectroscopic gas analysers, we observed consistent net foliar methane oxidation and nitrous oxide emission across all light conditions, demonstrating saturating light response patterns. Maximum flux rates were significantly more sensitive to soil conditions than carbon dioxide or water vapour exchange. Analysis revealed foliar methane and nitrous oxide fluxes overwhelmingly regulated by internal leaf processes like xylem transport, with modulation by external light intensity. These predictable light-response patterns provide a basis for scaling leaf-level methane and nitrous oxide fluxes, enhancing accuracy in predicting biogenic greenhouse gas fluxes within ecosystem and biosphere models.

Non-carbon dioxide (CO_2) biogenic greenhouse gases (GHGs), particularly methane (CH_4) and nitrous oxide (N_2O), contribute significantly to global anthropogenic climate forcing[1], with global warming potentials (GWP) 28 and 265 times higher than CO_2, respectively, over a 100-year timescale[2]. Although anthropogenic sources such as agriculture and industrial emissions dominate CH_4 and N_2O fluxes, natural ecosystems—including soils and vegetation—also play a crucial yet incompletely characterized role in global GHG budgets. Previous research[3–5] has demonstrated both CH_4 emission and uptake in tree stems[6] and forest soils[3,4]. Despite evidence that leaves can act as net sinks or sources of CH_4 and N_2O[7,8], foliar GHG exchange remains an underexplored pathway. Given the vast global surface area of foliage, even small fluxes could substantially influence atmospheric CH_4 and N_2O concentrations, underscoring the urgent need for empirical data to constrain these fluxes in climate models. However, the scarcity of experimental studies under varying environmental conditions hinders linking these foliar fluxes to tree physiological processes and soil characteristics, leaving regulatory mechanisms unresolved.

A key challenge in understanding foliar CH_4 and N_2O fluxes is identifying their environmental controls, particularly the role of light and transpiration in regulating these trace gases. Light quality and quantity strongly influence plant physiological and biochemical processes, with effects varying among species[9]. Light response curves (LCs) are a fundamental tool in plant eco-physiology[10], widely used to model photosynthetic activity and stomatal regulation[11,12]. Since stomatal conductance and transpiration are highly sensitive to light conditions, they may also influence the transport and diffusion of trace gases, including CH_4 and N_2O[13,14]. Characterizing LCs for foliar CH_4 and N_2O fluxes may offer critical insights into the physiological determinants of these fluxes and improve predictions of large-scale sources and sinks in global GHG budgets. Addtionally, relationships between CH_4 and N_2O fluxes and transpiration could clarify underlying mechanisms. Prior studies have focused primarily on soil, tree stem, and whole-plant CH_4 and N_2O emissions[4,15,16], lacking detailed data on leaf-level fluxes, especially regarding their modulation by light. Recent field surveys of foliar CH_4 and N_2O fluxes[7,17] have reported measurements at only a few discrete light intensities (e.g., 0, 100, and 1000 μmol·m^{-2}·s^{-1} PPFD), providing insufficient resolution to characterize the full light response.

While foliar gas exchange is influenced by light and transpiration dynamics, the internal mechanisms of leaf-level CH_4 oxidation remain underexplored, particularly under field-relevant conditions. Methanotrophic bacteria residing in or on plant leaves are hypothesized to drive CH_4 oxidation, potentially following saturating enzyme kinetics with CH_4 concentrations[18]. CH_4 in leaves can be supplied by two main pathways: dissolved CH_4 in the xylem stream, which generally scales with transpiration (E), and diffusion from the atmosphere into the leaf's internal airspace, which can saturate at high E rates. CH_4 oxidation by leaf surface methanotrophs is independent of E. Net atmospheric CH_4 uptake may occur

Institute of Forestry and Conservation, John H. Daniels Faculty of Architecture, Landscape, and Design, University of Toronto, 33 Willcocks Street, Toronto, ON, M5S 3B3, Canada. ✉e-mail: rezaul.karim@mail.utoronto.ca

when the equilibrium concentration within the leaf falls below the external CH_4 concentration[14].

Plant leaves can produce N_2O through microbial activity or internal physiological processes. Some studies suggest soil-derived N_2O transport, while others propose internal production via nitrate (NO_3^-) assimilation, with N_2O potentially forming from nitric oxide (NO) in mitochondria[13]. Excess soil nitrogen (N) can increase plant-derived N_2O emissions[19] by elevating N substrate availability (e.g., NO_3^-, NO_2^-), which is taken up by roots and leaves and reduced to N_2O. It remains unclear whether these reductions occur within plant cells or through endophytes[20,21]. N_2O release is linked to nitrate reductase (NR) activity, which increases with N inputs, enhancing plant growth and N_2O production[19,22].

Biochar, or charcoal designed for use as a soil amendment, is recognized for its potential to mitigate soil GHG emissions by enhancing soil aeration, with pronounced effects on N_2O and variable outcomes for CH_4[23]. Possible effects on foliar N_2O and CH_4 fluxes remain largely unexamined. By altering soil N availability, biochar may directly affect dissolved N_2O and CH_4 concentrations reaching leaves and indirectly modify foliar gas exchange through improved water and nutrient retention[24]. Such changes can influence stomatal conductance and photosynthetic rates, which are key regulators of foliar fluxes. However, biochar's impact on plant physiology varies with soil properties, application rate, and biochar characteristics[25,26]. Enhanced soil aeration under biochar amendment may increase CH_4 oxidation and reduce CH_4 production[27]. Similarly, improved soil aeration and modified N cycling due to biochar applications can reduce N_2O emissions, as the porous structure of biochar creates more space within the soil, facilitating air and water movement. However, outcomes depend on factors such as soil texture and organic carbon content[28]. Short-term reductions in nitrogen availability due to NH_4^+ binding, coupled with long-term improvements in soil structure and nutrient retention, suggest that biochar may lower foliar N_2O emissions by limiting nitrogen substrates[29–31]. Whether these soil-based mechanisms translate to altered foliar N_2O or CH_4 fluxes remains unexplored, underscoring the need for research on how biochar additions influence foliar CH_4 and N_2O fluxes.

This study examines the combined effects of N fertilization and biochar application on foliar CH_4 and N_2O fluxes, incorporating light-response curves and photosynthetic gas-exchange measurements. We take advantage of newly developed gas analyzers capable of high-frequency, real-time measurements of CH_4 and N_2O, integrated with a purpose-built cuvette system. Given that early successional species often exhibit higher gas flux rates (e.g. CO_2, H_2O), we selected *Salix bebbiana* (Bebb's willow) as our model species. Specifically, this study aims to: (i) characterize the light response curves of foliar CH_4 and N_2O fluxes; (ii) determine whether foliar CH_4 and N_2O fluxes are primarily regulated by internal plant processes rather than surface processes; and (iii) evaluate the effects of soil treatments with biochar and nitrogen fertilization on foliar CH_4 and N_2O exchange.

Results

Foliar CH_4 oxidation and N_2O emission show saturating light responses

The light response curve of foliar CH_4 oxidation exhibited a convex downward saturating pattern across all treatments, with generalized Poisson models providing the best fit, except for the biochar + low N treatment, which followed a non-rectangular hyperbolic model (Table 1). In the control, CH_4 oxidation reached a maximum light-saturated uptake ($P_{max}CH_4$) of 1.59 nmol·m^{-2}·s^{-1}, with a light saturation point (I_k) of 3018 μmol·m^{-2}·s^{-1} (Fig. 1a). Biochar increased $P_{max}CH_4$ to 2.73 nmol·m^{-2}·s^{-1}, while low and high N treatments reduced $P_{max}CH_4$ to 1.16 and 1.05 nmol·m^{-2}·s^{-1}, respectively (Fig. 1b). Biochar combined with low N exhibited a higher $P_{max}CH_4$ (1.73 nmol·m^{-2}·s^{-1}) compared to the low N treatment without biochar. In contrast, the biochar-high N combination resulted in a modest $P_{max}CH_4$ of 1.12 nmol·m^{-2}·s^{-1} (Fig. 1b). Net CH_4 oxidation was observed across all treatments, with dark condition (0 μmol·m^{-2}·s^{-1} PPFD) fluxes approaching zero but significantly deviated from zero ($Z = 6.98$, $p < 0.001$; Supplementary Fig. 1).

The sigmoid model best described the light response of foliar N_2O emissions in most treatments (Table 1). The maximum N_2O emission ($P_{max}N_2O$) was 0.113 pmol·m^{-2}·s^{-1} in control, with an irradiance midpoint (I_m) of 424.8 μmol·m^{-2}·s^{-1} (Fig. 1e). Biochar reduced $P_{max}N_2O$ to 0.087 pmol·m^{-2}·s^{-1}, while low N increased $P_{max}N_2O$ to 0.155 pmol·m^{-2}·s^{-1}, and high N further enhanced it to 0.263 pmol·m^{-2}·s^{-1} (Fig. 1f). In the biochar + low N treatment, N_2O emissions followed a generalized Poisson, with a $P_{max}N_2O$ of 0.146 pmol·m^{-2}·s^{-1} and a high light saturation point (I_k) of 2735 μmol·m^{-2}·s^{-1} (Fig. 1f). Similarly, the biochar + high N combination yielded a $P_{max}N_2O$ of 0.252 pmol·m^{-2}·s^{-1} and an I_k of 2324 μmol·m^{-2}·s^{-1} (Fig. 1f). N_2O effluxes were detected under all conditions, including in darkness. Z-tests confirmed that mean N_2O fluxes significantly deviated from zero under dark conditions ($Z = 6.10$, $p < 0.001$; Supplementary Fig. 1).

The net photosynthesis and transpiration rates across treatments were best characterized by the non-rectangular hyperbola model, which showed the best fit with the significance of model parameters and yielded the lowest values for both AIC and BIC (Table 1). The control achieved a maximum photosynthesis rate (P_{max}) of 29.75 μmol CO_2·m^{-2}·s^{-1}, which increased with biochar (35.54 μmol CO_2·m^{-2}·s^{-1}) (Fig. 1c) and low N treatment (32.60 μmol CO_2·m^{-2}·s^{-1}), whereas high N showed P_{max} of 30.57 μmol CO_2·m^{-2}·s^{-1} (Fig. 1d). For the combined treatments, biochar with low N showed a P_{max} of 28.66 μmol CO_2·m^{-2}·s^{-1}, while biochar with high N resulted a P_{max} of 29.90 μmol CO_2·m^{-2}·s^{-1}. These results indicate that biochar enhances net photosynthesis, with the effect modulated by N availability.

Furthermore, in the case of foliar transpiration, biochar increased the E_{max} from 138.95 μmol H_2O·m^{-2}·s^{-1} to 256.45 μmol H_2O·m^{-2}·s^{-1} (Fig. 1g). The low N treatment without biochar showed E_{max} of 145.36 μmol H_2O·m^{-2}·s^{-1}, while high N increased the E_{max} to 157.08 μmol H_2O·m^{-2}·s^{-1}. Biochar + low N resulted a E_{max} of 165.47 μmol H_2O·m^{-2}·s^{-1}, whereas with high N reached a E_{max} of 168.83 μmol H_2O·m^{-2}·s^{-1} (Fig. 1h). These results highlight the role of biochar in foliar transpiration, modulated by N application.

Biochar-enhanced CH_4 oxidation and reduced N_2O emissions offset by high N

The effects of soil treatments on foliar CH_4 oxidation at a standard light intensity (1000 μmol·m^{-2}·s^{-1} PPFD) were significant ($p < 0.001$) (Fig. 2a). The biochar treatment showed the highest CH_4 oxidation rate (0.642 ± 0.0103 nmol·m^{-2}·s^{-1}), significantly ($p < 0.001$) higher than the control (0.444 ± 0.02 nmol·m^{-2}·s^{-1}). Furthermore, low N (0.350 ± 0.005 nmol·m^{-2}·s^{-1}) and high N (0.277 ± 0.005 nmol·m^{-2} s^{-1}) reduced the CH_4 oxidation compared to the control ($p < 0.001$). However, no significant difference ($p = 0.448$) was found between the biochar + low N treatment (0.412 ± 0.004 nmol·m^{-2}·s^{-1}) and the control, while the biochar + high N treatment (0.318 ± 0.009 nmol m^{-2} s^{-1}) was significantly lower ($p < 0.001$) than the control. Additionally, overall soil treatment effects on soil CH_4 oxidation were significant ($p < 0.001$) (Fig. 2b). Biochar increased CH_4 oxidation to 0.489 ± 0.0142 nmol m^{-2} s^{-1}, significantly ($p < 0.001$) higher than the control (0.423 ± 0.0114 nmol·m^{-2}·s^{-1}). On the other hand, both low N (0.233 ± 0.009 nmol·m^{-2}·s^{-1}) and high N (0.143 ± 0.010 nmol·m^{-2}·s^{-1}) significantly ($p < 0.001$) reduced CH_4 oxidation compared to the control.

The effects of soil treatments on foliar N_2O emissions were significant overall ($p < 0.001$) (Fig. 2c). N_2O emissions in the control treatment were 0.0938 ± 0.00284 pmol·m^{-2}·s^{-1}, while biochar significantly reduced the emission rate to 0.0683 ± 0.00176 pmol·m^{-2}·s^{-1} ($p < 0.01$). Low N (0.142 ± 0.00219 pmol·m^{-2}·s^{-1}), and high N (0.236 ± 0.00554 pmol·m^{-2}·s^{-1}) treatments increased foliar N_2O emissions,where the high N significantly ($p < 0.05$) more than the low N treatment. Biochar + low N further showed an emission of 0.103 ± 0.000531 pmol·m^{-2}·s^{-1}, while high N exhibited a value of 0.222 ± 0.00689 pmol·m^{-2}·s^{-1}. Overall, while biochar application

Table 1 | Best-fit model parameters for light-response curves

Gas	Treatment	Model	Parameter	Value
CH_4	Control	Generalized Poisson	P_{maxCH_4}	1.593
			I_k	3018.3
			n	0.783
	Biochar	Generalized Poisson	P_{maxCH_4}	2.731
			I_k	2960.3
			n	0.976
	Low N	Generalized Poisson	P_{maxCH_4}	1.156
			I_k	1720
			n	1.232
	High N	Generalized Poisson	P_{maxCH_4}	1.053
			I_k	1926
			n	1.203
	Biochar + Low N	Non-rectangular hyperbola	P_{maxCH_4}	1.739
			α	0.011
			θ	−86.87
	Biochar + High N	Generalized Poisson	P_{maxCH_4}	1.127
			I_k	1285
			n	0.457
CO_2	Control	Non-rectangular hyperbola	P_{max}	29.757
			α	0.053
			θ	0.799
	Biochar	Non-rectangular hyperbola	P_{max}	35.543
			α	0.111
			θ	0.004
	Low N	Non-rectangular hyperbola	P_{max}	32.605
			α	0.035
			θ	0.872
	High N	Non-rectangular hyperbola	P_{max}	30.578
			α	0.070
			θ	0.585
	Biochar + Low N	Non-rectangular hyperbola	P_{max}	28.659
			α	0.068
			θ	0.735
	Biochar + High N	Non-rectangular hyperbola	P_{max}	29.902
			α	0.078
			θ	0.430
N_2O	Control	Sigmoid	P_{maxN_2O}	0.1134
			I_m	424.8
			k	288.2
	Biochar	Sigmoid	P_{maxN_2O}	0.0873
			I_m	612.5
			k	274.0
	Low N	Hyperbola	P_{maxN_2O}	0.166
			I_k	187.3
	High N	Smith	P_{maxN_2O}	0.284
			α	0.0006
			θ	−1.665
			R_d	−0.079
	Biochar + Low N	Generalized Poisson	P_{maxN_2O}	0.2841
			I_k	2735
			n	0.6570
	Biochar + High N	Generalized Poisson	P_{maxN_2O}	0.5231
			I_k	2324
			n	0.4096
H_2O	Control	Non-rectangular hyperbola	E_{max}	138.953
			α	0.342
			θ	0.828
	Biochar	Non-rectangular hyperbola	E_{max}	256.454
			α	0.413
			θ	0.854
	Low N	Non-rectangular hyperbola	E_{max}	145.361
			α	0.341
			θ	0.901
	High N	Non-rectangular hyperbola	E_{max}	157.075
			α	0.295
			θ	0.920
	Biochar + Low N	Non-rectangular hyperbola	E_{max}	165.465
			α	0.296
			θ	0.807
	Biochar + High N	Non-rectangular hyperbola	E_{max}	168.834
			α	0.275
			θ	0.871

All parameters reported are statistically significant ($p < 0.05$).

reduced N_2O emissions, high N application increased emissions rate. Furthermore, the overall soil treatment effects on soil N_2O emissions were significant ($p < 0.001$) (Fig. 2d). The control showed a mean N_2O emission of 0.0836 ± 0.008 pmol·m^{-2}·s^{-1}, while biochar reduced emissions to 0.0350 ± 0.008 pmol·m^{-2}·s^{-1}, but this difference was not statistically significant ($p = 0.919$). In contrast, treatments with low N (1.04 ± 0.0157 pmol·m^{-2}·s^{-1}) showed significantly ($p < 0.001$) lower emission than high N (1.59 ± 0.0766 pmol·m^{-2}·s^{-1}). Biochar + low N (0.628 ± 0.0255 pmol·m^{-2}·s^{-1}) and high N (0.907 ± 0.0212 pmol·m^{-2}·s^{-1}) also significantly ($p < 0.01$) reduced N_2O emissions ($p < 0.001$) compared to low N and high N, respectively.

In the absence of light (0 μmol·m^{-2}·s^{-1} PPFD), minimal but detectable, amounts of foliar CH_4 oxidation and N_2O emission were observed. Significant differences were found in CH_4 oxidation between the control and biochar treatments, as well as in foliar N_2O emissions between the low N and high N treatments (Supplementary Fig. 1a, b).

Foliar CH_4 and N_2O fluxes in relation to transpiration

The relationship between foliar CH_4 oxidation, N_2O emissions, and transpiration varied across different soil treatments (Fig. 3). CH_4 oxidation showed an exponential relationship with transpiration in the control (RSE = 0.061, $p < 0.001$; Fig. 3a), and biochar (RSE = 0.072, $p < 0.001$; Fig. 3b) treatments. In the low N treatment, a sigmoidal relationship was observed between transpiration and CH_4 oxidation (RSE = 0.062, $p < 0.001$), while an exponential model fit the relationship for high N (RSE = 0.045, $p < 0.001$; Figs. 3c, d). The addition of N with biochar followed BET models (RSE = 0.034 for low N and 0.028 for high N, $p < 0.001$) (Figs. 3e, f). For foliar N_2O emissions, the control treatment followed an Aguerre–Suarez–Viollaz (ASV) model (RSE = 0.010, $p < 0.001$; Fig. 3g). The biochar treatment (Fig. 3h) and the low N treatment (Fig. 3i) were best represented by exponential models (RSE = 0.005 and 0.012, respectively; $p < 0.001$). In contrast, the high N treatment (RSE = 0.019, $p < 0.001$; Fig. 3j) and the biochar + high N treatment (RSE = 0.015, $p < 0.001$; Fig. 3k) were

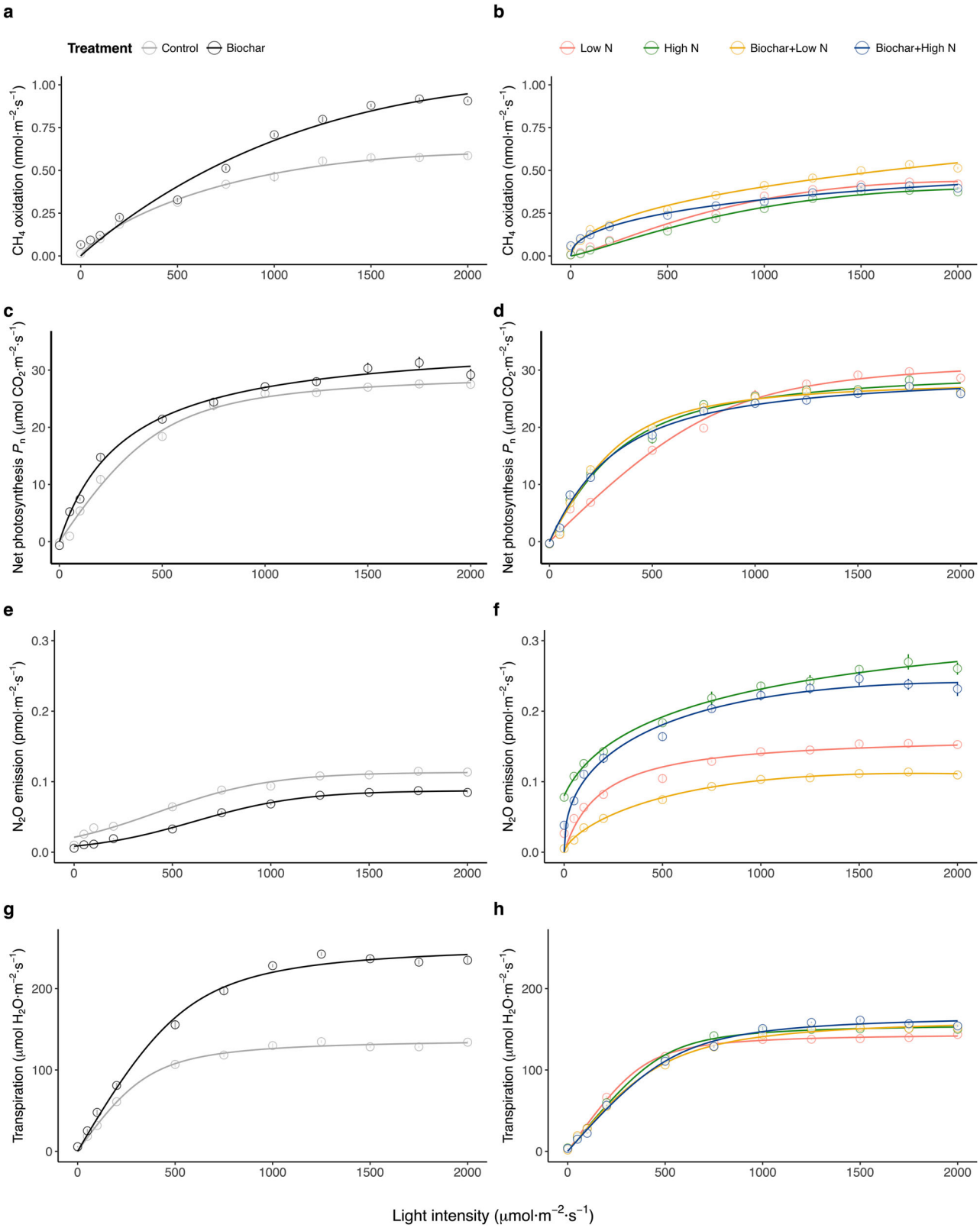

Fig. 1 | Light response curves of foliar gas exchange under different soil treatments. Panels (**a**, **b**) show foliar CH_4 oxidation (nmol·m^{-2}·s^{-1}), (**c**, **d**) net photosynthesis (μmol CO_2 ·m^{-2}·s^{-1}), (**e**, **f**) N_2O emission (pmol·m^{-2}·s^{-1}), and (**g**, **h**) transpiration (μmol H_2O·m^{-2}·s^{-1}) with light intensity under 0, 50, 100, 200, 500, 750, 1000, 1250, 1500, 1750, and 2000 μmol·m^{-2}·s^{-1}. The "control" refers to plants in pots with soil only, without any amendments. Data are shown for leaf surface flux measurements for all treatments.

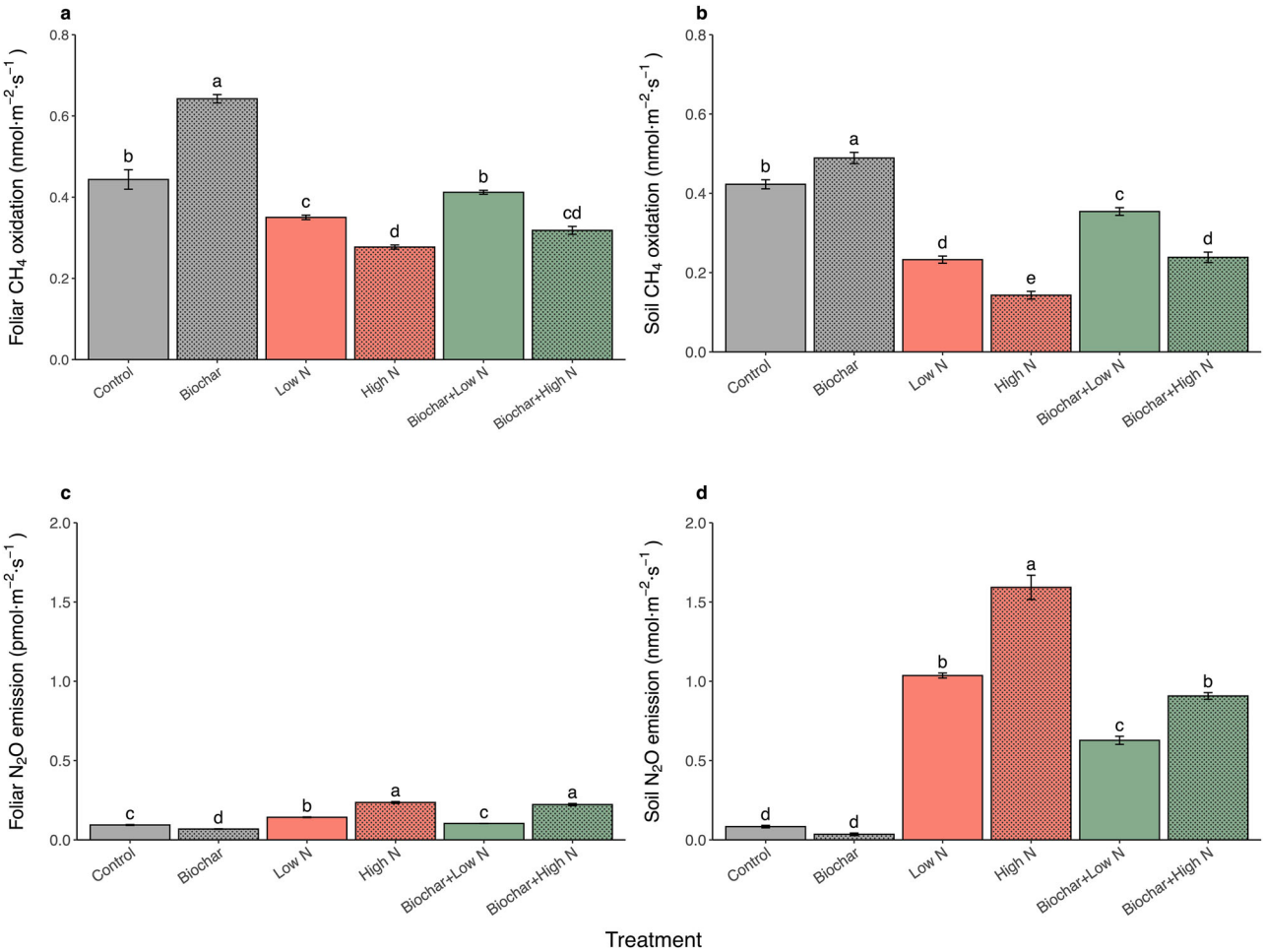

Fig. 2 | Effects of soil amendment treatments on foliar and soil gas fluxes. Panels (**a**) and (**c**) show foliar CH_4 oxidation (nmol·m^{-2}·s^{-1}) and N_2O emission (pmol·m^{-2}·s^{-1}), respectively, measured under a light intensity of 1000 μmol·m^{-2}·s^{-1} photosynthetic photon flux density (PPFD). Panels (**b**) and (**d**) show soil CH_4 oxidation and N_2O emission (nmol and pmol·m^{-2}·s^{-1}, respectively). Bars represent mean values ± standard error (SE). Different letters above bars indicate statistically significant differences among treatments ($p < 0.05$).

optimally described by ASV models. In the biochar + low N treatment, a BET model (RSE = 0.005; $p < 0.001$) effectively captured the positive relationship (Fig. 3l).

Leaf surface vs. internal sources of foliar CH_4 oxidation and N_2O emissions

The analysis revealed detectable amounts of CH_4 and N_2O, with treatment-dependent variations that were independent of transpiration and xylem-mediated transport of soil-derived dissolved gases in the transpiration stream (Fig. 3; linear model). At zero transpiration, CH_4 oxidation rates were significantly above zero ($p < 0.05$) as follows: biochar (0.045 ± 0.01 nmol·m^{-2}·s^{-1}, 1.65% of $P_{max}CH_4$; 95% CI: [0.024, 0.066]), biochar + low N (0.03 ± 0.01 nmol·m^{-2}·s^{-1}, 1.73% of $P_{max}CH_4$; 95% CI: [0.015, 0.06]) and biochar + high N (0.05 ± 0.01 nmol·m^{-2}·s^{-1}, 4.46% of $P_{max}CH_4$; 95% CI: [0.024, 0.077]). However, no CH_4 oxidation was detected as significantly different from zero ($p > 0.05$) under control (0.013 ± 0.009 nmol m^{-2} s^{-1}, 0.82% of $P_{max}CH_4$; 95% CI: [−0.005, 0.033]), low N (0.003 ± 0.0033 nmol m^{-2} s^{-1}, 0.26% of $P_{max}CH_4$; 95% CI: [−0.003, 0.009]), and high N (−0.004 ± 0.002 nmol·m^{-2}·s^{-1}, −0.38% of $P_{max}CH_4$; 95% CI: [−0.01, 0.001]) treatments.

Regarding foliar N_2O emissions at zero transpiration, significantly non-zero ($p < 0.05$) emissions were observed in control (0.006 ± 0.001 pmol·m^{-2}·s^{-1}, 0.11% of $P_{max}N_2O$; 95% CI: [0.002, 0.011]), biochar (0.005 ± 0.0009 pmol·m^{-2}·s^{-1}, 0.09% of $P_{max}N_2O$; 95% CI: [0.004, 0.008]) and low N (0.02 ± 0.002 pmol·m^{-2}·s^{-1}, 0.15% of $P_{max}N_2O$; 95% CI: [0.015, 0.027]), high N (0.07 ± 0.004 pmol·m^{-2}·s^{-1}, 0.26% of $P_{max}N_2O$; 95% CI: [0.062, 0.079]) treatments and biochar + high N (0.02 ± 0.006 pmol·m^{-2}·s^{-1}, 0.25% of $P_{max}N_2O$; 95% CI: [0.011, 0.038]). In contrast, no detectable N_2O emission at zero transpiration was observed in the biochar + low N (0.002 ± 0.002 pmol·m^{-2}·s^{-1}, 0.15% of $P_{max}N_2O$; 95% CI: [−0.003, 0.007]) treatment.

Correlations of foliar CH_4 and N_2O fluxes with soil fluxes and leaf traits

We assessed how foliar CH_4 oxidation and N_2O emission relates to soil CH_4 and N_2O fluxes, as well as to leaf traits (leaf total nitrogen and specific leaf area) using model fitting based on residual standard error (RSE) and selection criteria including the AIC and BIC for linear and non-linear models. Foliar CH_4 oxidation showed a positive quadratic relationship with soil CH_4 oxidation (adjusted $r^2 = 0.84$, $p < 0.001$) (Fig. 4a) and a significant negative linear relationship with leaf total N (%) ($r^2 = 0.51$, $p < 0.001$) (Fig. 4b). An exponential relationship with specific leaf area (SLA) was observed (adjusted $r^2 = 0.12$, $p < 0.05$) (Fig. 4c). No significant association with soil total N (%) was determined in our study ($p > 0.05$).

Foliar N_2O emission showed positive linear relationship with soil N_2O emission ($r^2 = 0.74$, $p < 0.001$) (Fig. 4d) and a significant positive quadratic association with leaf total N (%) ($r^2 = 0.84$, $p < 0.001$) (Fig. 4e). However, no

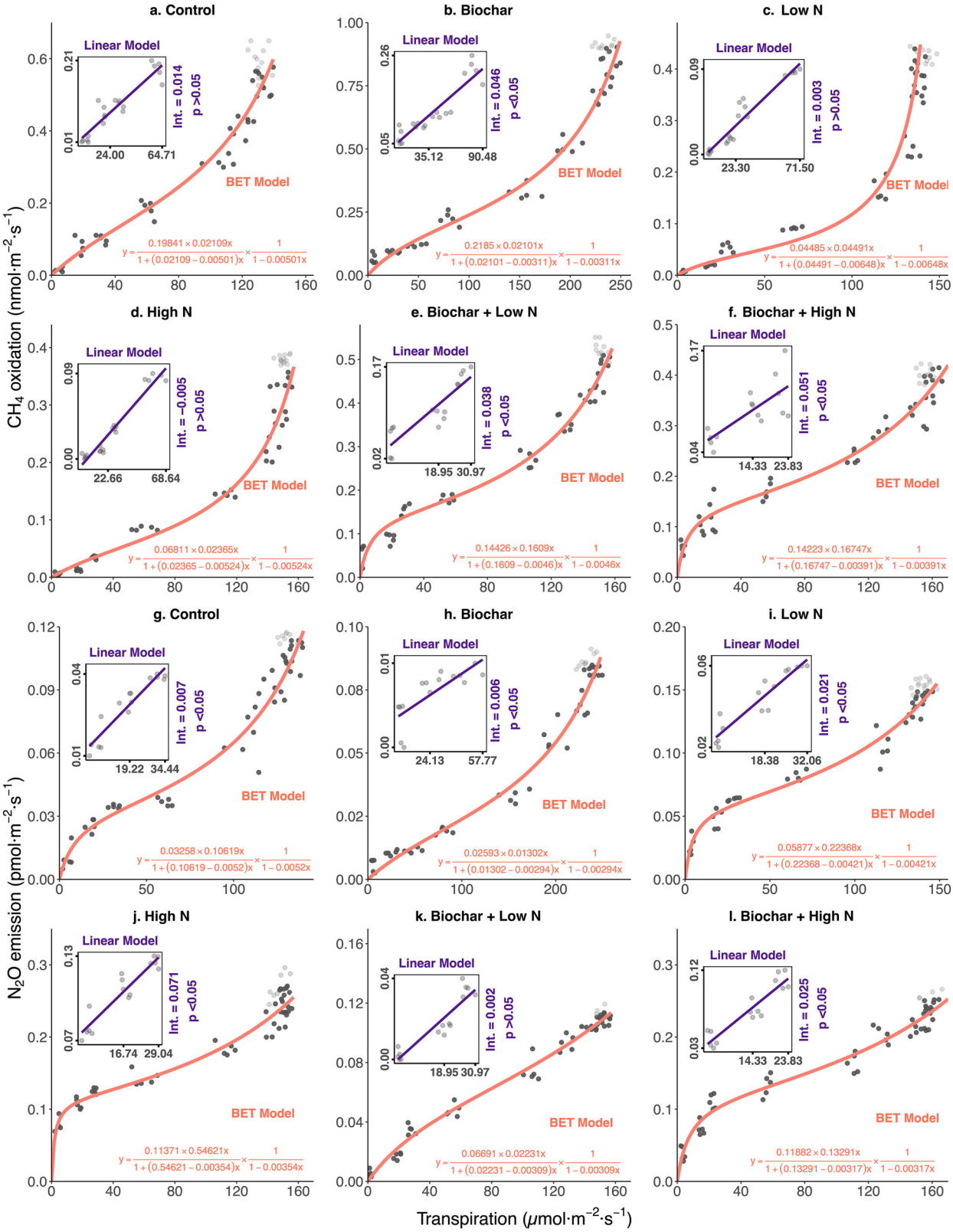

Fig. 3 | Relationships between foliar gas fluxes and transpiration under different soil treatments. Panels (**a**–**f**) show relationships between transpiration rates (μmol $H_2O{\cdot}m^{-2}{\cdot}s^{-1}$) and CH_4 oxidation (nmol $CH_4{\cdot}m^{-2}{\cdot}s^{-1}$), while panels (**g**–**l**) display relationships between transpiration and N_2O emission (pmol $N_2O{\cdot}m^{-2}{\cdot}s^{-1}$), across six soil treatment combinations: (**a**, **g**) control (unamended soil), (**b**, **h**) biochar, (**c**, **i**) low nitrogen, (**d**, **j**) high nitrogen, (**e**, **k**) biochar + low nitrogen, and (**f**, **l**) biochar + high nitrogen. Each panel includes a linear regression fit describing the relationship between gas flux and transpiration. Insets labeled "Int." display intercept-only models, representing baseline gas fluxes at zero transpiration. All symbols, line styles, and colors are defined in the corresponding figure legend.

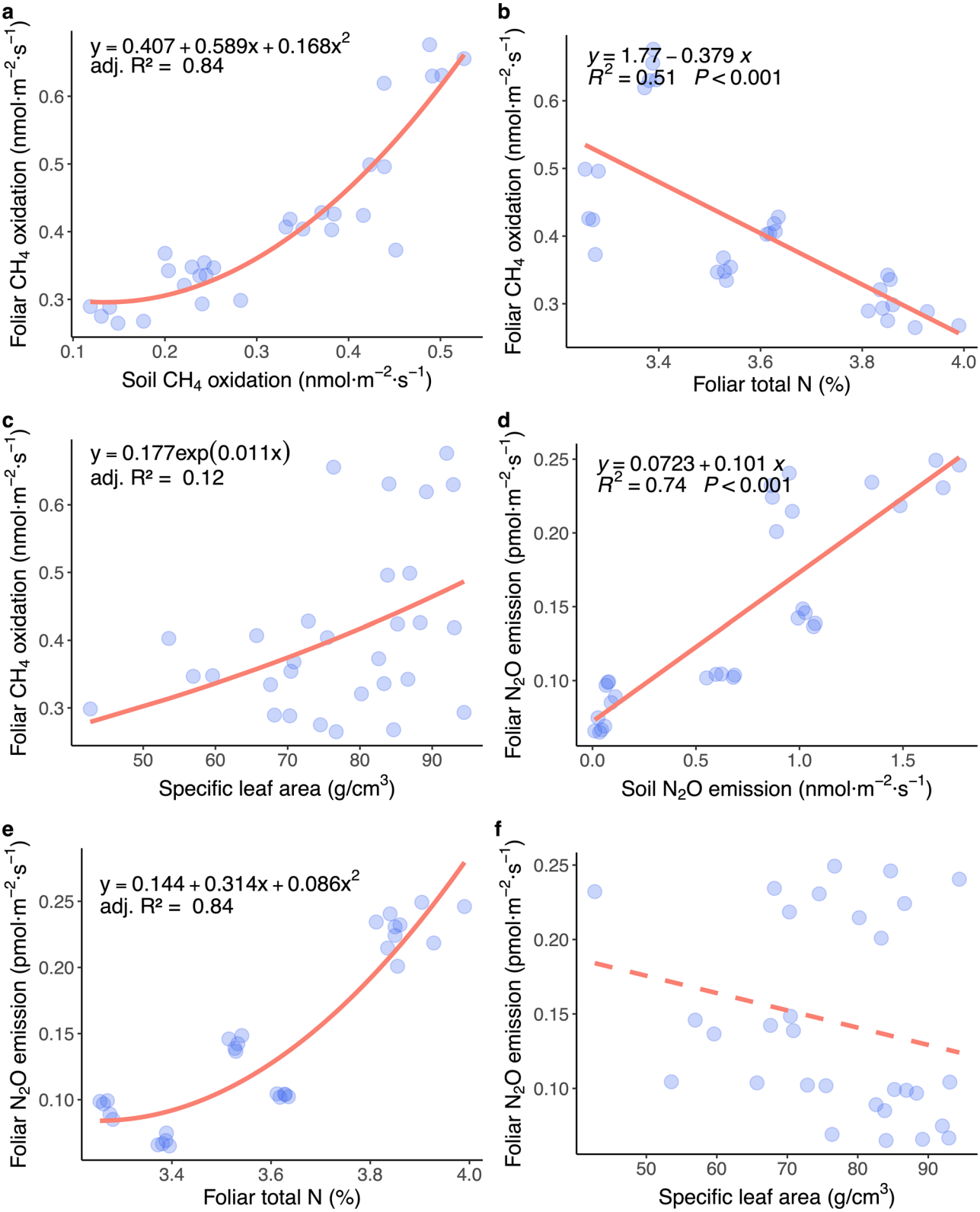

Fig. 4 | Relationships between foliar gas fluxes and biophysical or biogeochemical factors. Panels (**a**–**c**) show relationships between leaf CH_4 oxidation rates (nmol·m^{-2}·s^{-1}) and (**a**) soil CH_4 oxidation (nmol·m^{-2}·s^{-1}), (**b**) leaf total nitrogen content (%), and (**c**) specific leaf area (SLA; g cm^{-3}). Panels (**d**–**f**) present relationships between leaf N_2O emission rates (pmol·m^{-2}·s^{-1}) and (d) soil N_2O emission (nmol·m^{-2}·s^{-1}), (**e**) leaf total nitrogen content (%), and (**f**) SLA (g cm^{-3}). Solid lines represent statistically significant linear relationships ($p < 0.05$), while dashed lines indicate non-significant relationships.

significant relationships were observed between foliar N_2O emission and either SLA (Fig. 4e) or soil total N (%) ($p > 0.05$).

Discussion

Results indicated that CH_4 and N_2O fluxes are highly responsive to light conditions, exhibiting predictable light-response curves for these gases described here for the first time. Notably, N_2O efflux followed a sigmoidal form, being convex at low light levels. Strong relationships were observed between CH_4 and N_2O fluxes and transpiration, though all were non-linear, suggesting the importance of non-stomatal light-responsive processes. By estimating fluxes at zero transpiration, our findings also distinguish leaf surface from internal processes, revealing small but detectable leaf surface exchange of CH_4 and N_2O. Light-response curves for CH_4 and N_2O were remarkably responsive to soil conditions, much more so than CO_2 or water vapor.

Our results highlight the importance of distinguishing between surface-level processes and internal methanotrophic activity in regulating CH_4 fluxes. Linear-model intercepts were significantly different from zero under biochar treatments, implying some surface-driven CH_4 uptake; however, in all treatments this was a small fraction of fluxes observed under high-light conditions. Enhanced stomatal conductance under higher light[32] necessarily enhances CH_4 diffusion into leaves, pointing to an indirect influence of light via stomatal opening rather than a direct effect on methanotrophs. Since temperature, relative humidity, and boundary layer conductance were maintained at near-constant levels during measurements, their confounding effects on transpiration rates and CH_4 uptake were minimized. Therefore, the observed patterns in foliar CH_4 uptake are most likely driven by light intensity and its interaction with physiological processes, particularly stomatal regulation and potential internal CH_4 transport mechanisms.

A sigmoidal model effectively described the N_2O emission responses to light with an initial convex rise at low-moderate light—likely reflecting light-driven biochemical pathways associated with nitrogen metabolism—followed by a non-linear surge above 1500 $\mu mol \cdot m^{-2} \cdot s^{-1}$, eventually approaching a plateau. This pattern suggests that while stomatal conductance may facilitate N_2O release under increasing light, internal metabolic controls become dominant at higher irradiance levels.

Elevated light levels increase stomatal conductance, both directly and indirectly, through changes in intercellular CO_2 concentration[33,34]. This increase in stomatal conductance could facilitate N_2O release from leaves, especially under high nitrogen availability, as observed in previous studies[19,21]. Furthermore, at higher light levels, enhanced photosynthesis may increase nitrogen assimilation[35]. However, as photosynthetic rates in our study saturated around 1500 $\mu mol \cdot m^{-2} \cdot s^{-1}$, nitrogen assimilation does not directly correlate with net photosynthetic carbon fixation. This indicates that other factors, such as changes in nitrogen metabolism or the accumulation of nitrogen intermediates like nitrite (NO_2^-), must contribute to the observed increase in N_2O emissions at higher light intensities (>1500 $\mu mol \cdot m^{-2} \cdot s^{-1}$). These findings suggest a more complex interaction between very high light intensity, photosynthesis, and nitrogen cycling in regulating N_2O emissions.

Excessive accumulation of NO_2^- in higher light can lead to its partial conversion into nitrous oxide (N_2O) through incomplete reduction pathways[20], likely explaining the non-linear N_2O increase at high light and transpiration. Under normal light intensity, when green leaves are exposed to light, the enzyme glucose-6-phosphate dehydrogenase is inhibited by reduction via thioredoxin. Consequently, the dark nitrate assimilation pathway is suppressed under photoautotrophic conditions and substituted by regulatory reactions that function in light. Due to the direct photosynthetic reduction of nitrite (NO_2^-) in chloroplasts and the availability of excess NADH for nitrate reductase (which catalyzes the reduction of NO_3^- to NO_2^-), the rate of nitrate assimilation is significantly enhanced under light conditions[36].

Soil treatments (biochar and N fertilizer amendments) had pronounced effects on foliar CH_4 and N_2O fluxes compared to CO_2 or H_2O fluxes. Biochar enhanced CH_4 oxidation and reduced N_2O emissions, whereas N fertilizer increased N_2O emissions and curtailed CH_4 oxidation. Biochar likely promotes CH_4 oxidation by improving soil water retention[37], leading to increased transpiration and enabling atmospheric CH_4 to enter leaves, where endophytic methanotrophs can act[38,39]. Still, the non-linear, upwardly convex relationship between foliar CH_4 oxidation and transpiration (E) at high light levels suggests mechanisms beyond simple diffusion.

By contrast, N fertilization reduced foliar CH_4 uptake. While no direct association between N fertilization and foliar CH_4 uptake has previously been reported in the literature, prior research suggests that NH_4^+ and CH_4 share comparable structures and sizes, allowing certain methanotrophs, particularly those utilizing particulate methane monooxygenase (pMMO), to co-oxidize both compounds[40]. Since methanotrophs primarily rely on CH_4 as their carbon and energy source, an increase in NH_4^+ concentrations may directly reduce CH_4 oxidation[41]. The preferential oxidation of NH_4^+ by methanotrophs using pMMO occurs when NH_4^+ is available at higher concentrations, displacing CH_4 as the primary substrate. This process is particularly pronounced in upland soils, where lower CH_4 concentrations coexist with oxygen, resulting in reduced CH_4 uptake[42]. While this mechanism is well-established in soil[43], its relevance to foliar CH_4 uptake remains uncertain. The reduction of nitrate to ammonium in plant leaves—facilitated by nitrate reductase (NR) and nitrite reductase (NiR)—may not directly expose endophytic methanotrophs in leaves to increased NH_4^+ concentrations. In addition, the presence of pMMO-expressing methanotrophs in leaves has not been definitively established, and there is even evidence for novel monooxygenases in leaf-inhabiting methanotrophs[44]. On the other hand, N fertilization significantly increased foliar N_2O emissions in plants in our study, likely due to enhanced nitrogen substrates elevating plant metabolic activity. Prior studies suggest that whole-plant or shoot-level N_2O emissions can more than double with N fertilization[8,19]. A key mechanism involves increased NO_3^- uptake by plant roots, which stimulates NR activity, reducing NO_3^- to NO_2^-; a portion of this NO_2^- is subsequently converted to N_2O[22]. In some plants, NR activity is confined to the roots, but in most trees, NR also occurs in the leaves[45], implying that higher foliar NR activity could further elevate foliar N_2O emissions. Our results also indicate that biochar amendment generally reduces foliar N_2O emissions. Biochar can enhance plant growth and photosynthesis by increasing chlorophyll content and stomatal conductance[29]; yet in the short term, it often reduces soil N availability by binding NH_4^+[30]. Over the long term, biochar improves soil structure and nutrient retention, enhancing nutrient use efficiency and reducing N leaching[31]. Consequently, lower foliar N_2O emissions likely result from both reduced NH_4^+ availability in the soil and diminishing foliar N status, which together limit N substrates that fuel foliar N_2O production.

The light-response curves developed in this study provide a potentially valuable tool for scaling leaf-level CH_4 and N_2O fluxes to broader ecological contexts by capturing the dynamic interplay between light intensity and gas fluxes. This should facilitate more accurate GHG emission predictions under diverse environmental conditions. This approach is similar to that taken with isoprene and monoterpene (MT) emissions, where light-response curves improve canopy-scale prediction of volatile organic compound (VOC) emissions[46,47], partly by incorporating plant-specific light and temperature responses[48]. Similarly, integrating light-dependent CH_4 and N_2O flux data into large-scale GHG models could substantially enhance landscape-level emission estimates. Although leaf-level processes show promise for larger-scale modeling, effectively scaling them to the ecosystem level requires careful consideration of localized factors such as soil nutrient availability and hydrology. Our results indicate that soil manipulations exerted far greater influence on foliar CH_4 and N_2O fluxes than on CO_2 fluxes. Hence, future modeling efforts should integrate leaf-level response curves within the context of soil processes to improve flux estimates in managed ecosystems as these estimates are crucial for optimizing GHG emission reductions[49]. Given the wide variation in foliar CH_4 uptake and N_2O emissions across species, a more comprehensive estimate of global

foliar fluxes would require a weighted average of flux rates across different forest types and regions. For instance, tropical, temperate, and boreal forests each contribute species with varying flux characteristics. Our findings suggest that biochar additions to forest soils would enhance foliar CH_4 uptake and reduce N_2O emissions, but scaled estimates are essential to evaluate their full mitigation potential. Such upscaled estimates could then be compared with direct soil-based flux estimates, like those from Saunois et al.[50], providing a more accurate representation of foliar processes' contribution to the global GHG budget. The present results were obtained using low-nutrient silty clay loam from an excavation site, typical to that colonized by the *S. bebbiana*. Further studies of later-successional species on intact forest soils across various regions are necessary to assess the broader generalization of these results.

This study presents the first characterization of leaf-level light-response curves for CH_4 and N_2O fluxes, revealing strong and predictable effects on foliar CH_4 uptake and N_2O emissions. Transpiration emerged as a key driver of CH_4 oxidation in leaves, while nitrogen assimilation influenced modulation of N_2O emissions. Although leaf surface processes contributed to CH_4 uptake and N_2O emissions under conditions of zero transpiration in some cases, the dominant controls were internal mechanisms, including xylem-mediated transport and microbial activity. Soil amendments significantly altered these dynamics: biochar enhanced CH_4 uptake and reduced N_2O emissions, whereas nitrogen fertilization had the opposite effect, decreasing CH_4 uptake and increasing N_2O emissions. These results highlight the importance of integrating light-dependent physiological processes into ecosystem and global GHG models to refine predictions of plant-mediated GHG exchange. Effects of temperature and other environmental parameters will be important steps in future studies. By elucidating the interplay between physiological and soil-mediated controls on foliar CH_4 and N_2O fluxes, this study advances understanding of the role of tree foliage in atmospheric GHG regulation, providing a foundation for future research aimed at plant-driven fluxes for climate adaptation and mitigation strategies.

Methods

Plant material

Salix bebbiana Sarg. (Bebb's willow) is widespread pioneer tree species across North America, thriving in both temperate and boreal ecosystems[51]. Its adaptability to various soil types and environmental conditions renders it a suitable model species for studying plant physiological responses to environmental change[52]. Moreover, the species' rapid growth and high leaf production facilitate efficient measurements of foliar greenhouse gas (GHG) fluxes[53]. In greenhouse settings, *S. bebbiana* requires minimal maintenance, increasing its practicality for controlled experiments.

S. bebbiana cuttings, ranging from 9.9 cm to 15.32 cm in length were collected from Tin Beaches Road South, Tiny, Ontario (44°40′56.62″ N–79°57′7.67″ W). Immediately after collection, cuttings were immersed in water to prevent desiccation and placed in a greenhouse at the University of Toronto, ON, Canada. They were kept in a water-filled container covered with a polythene wrap to maintain high relative humidity. Rooting hormone was not applied as *S. bebbiana* can root in water without supplementation. The water in the container was replaced every four days. After 15 days, a subset of cuttings had developed small roots; by 20 days, nearly 95% had produced rots and initiated leaf development.

Soil collection

Soil was collected from Downsview Park in Toronto, Ontario, Canada (43°44′34.50″ N −79°28′1.31″ W). The soil was primarily collected from an urban subway excavation site and exhibited low levels of essential nutrients (Supplementary Table 1).

Biochar production and characterization of physiochemical properties

The biochar used in this experiment was produced from sugar maple (*Acer saccharum* L.) sawdust via slow pyrolysis at ~700 °C with a residence time of ~10 min, supplied by Haliburton Biochar Ltd., Haliburton, ON, Canada. The total carbon C and nitrogen N contents (mass-based percentages) in the biochar were determined through combustion analysis. In brief, 2 mg of oven-dried, finely ground samples were analyzed using a LECO 628 CN analyzer (LECO Corporation, St. Joseph, MI, USA). Elemental compositions (Al, Ag, As, Au, Ba, Be, Bi, Ca, Cd, Ce, Co, Cr, Cu, Cs, Fe, Hf, K, La, Li, Na, Nb, Ni, P, Rb, Pb, S, Mg, Mn, Mo, Sb, Sc, Sn, Sr, Ta, Th, Ti, U, V, W, Y, and Zn) were quantified on oven-dried samples by inductive coupled plasma mass spectrometry (ICP-MS) at Activation Laboratories Ltd. (Ancaster, ON, Canada). The samples were ground to a fine powder, subjected to four-acid digestion (hydrofluoric, nitric, and perchloric acids), and then solubilized using nitric and hydrochloric acids. Biochar pH and electrical conductivity (EC) were measured after 24 h of shaking a 1:3 biochar-to-de-ionized water mixture with an Orion Star A112 Benchtop pH/EC meter (Thermo Fisher Scientific, Waltham, MA, USA). The physicochemical properties of the biochar are detailed in Table 2.

Table 2 | Physiochemical properties of Sugar maple (*Acer saccharum* Marsh.) biochar

Properties	Value (mean ± SE) (n = 3)	Unit
pH (H_2O)	7.87 ± 0.05	–
Electrical conductivity	62.72 ± 3.46	μS cm^{-1}
Total C	78.29 ± 0.30	%
N	0.43 ± 0.00	%
C:N ratio	182.07	–
P	0.0337 ± 0.0039	%
K	0.40 ± 0.03	%

Biochar was produced at a maximum temperature ~700 °C using a kiln-based method.
Notes: Additional elemental and trace metal properties of the biochar are provided in Supplementary Table 8.

Treatment and experimental design

A randomized block design was employed with six treatments: (1) a control group (no amendments), (2) low nitrogen (N) fertilizer (42 kg ha^{-1}), (3) high N fertilizer (75 kg ha^{-1}), (4) biochar (20 t ha^{-1}), (5) biochar plus low N (20 t ha^{-1} + 42 kg ha^{-1}), and (6) biochar plus high N (20 t ha^{-1} + 75 kg ha^{-1}). To avoid potential toxicity associated with urea [$CO(NH_2)_2$], ammonium sulfate [$(NH_4)_2SO_4$]—which contains 21% total N and no phosphorous or potassium—was used as the N source in our study. Biochar was applied as a solid and thoroughly mixed into the upper 10 cm of soil at an equivalent surface dose of 20 t ha^{-1}, corresponding to approximately 106.2 g per pot. N fertilizer was dissolved in deionized (DI) water and applied as a solution. The same volume of DI water was also added to control pots to standardize moisture inputs across treatments. Each pot measured 26 × 26 × 20.5 cm and received 5.5 kg of homogenized soil, with soil moisture was routinely monitored and adjusted to maintain consistency across all treatments.

The greenhouse experiment included five blocks, with each of six treatments randomly assigned within each block, resulting in 30 planted pots (6 treatments × 5 replicates). To evaluate soil GHG flux in the absence of vegetation, additional pots (also replicated five time per selected treatment) were prepared with *S. bebbiana*.

Foliar and soil gas-exchange

Until recently, static chamber approaches coupled with gas chromatography have been the primary tools for measuring CH_4 and N_2O fluxes in plant and soil studies[15,54]. However, these methods are not well-suited for in-situ measurements of low flux rates. In recent years, high-precision portable analyzers have enabled greater accuracy. In this study, we used an off-axis integrated cavity output spectroscopy (LGR 915-0011; Los Gatos, San Jose, CA, USA) for CO_2, CH_4, and H_2O, along with optical feedback–cavity enhanced absorption spectroscopy analyzer (LI-7820; Lincoln, Nebraska, USA), specifically designed for in-situ N_2O measurements.

Prior foliar flux measurements have often relied on static leaf chambers lacking controlled air flow and mixing, temperature, and relative humidity[55], which can reduce stomatal conductance[56]. Some studies have used detached foliage (e.g., Qin et al.[8]), potentially introducing large variable biases in gas-exchange measurements[57]. Others have adapted soil chambers to measure intact leaves[17], but the large chamber volume and limited control of leaf boundary layer conditions can compromise accuracy. Here, we used a newly developed dynamic leaf chamber (CS-LC7000, CredoSense Inc., Toronto, Ontario, Canada) to ensure a stable and controlled micro-environment with continuous air flow around the leaf (Supplementary Fig. 2). The system operated in a closed-dynamic loop, with an automated valve system allowing three one-minute measurements over a five-minute window. This system ensures complete air exchange within 60 s, preventing trace gas buildup and maintain near-ambient CO_2 and H_2O levels. A full-spectrum photodiode light source capable of delivering 0–2500 $\mu mol \cdot m^{-2} \cdot s^{-1}$ photosynthetic photon flux density (PPFD) was integrated into the chamber.

We measured foliar CH_4 and N_2O fluxes at PPDF levels of 0, 50, 100, 200, 500, 750, 1000, 1250, 1500, 1750, and 2000 $\mu mol \cdot m^{-2} \cdot s^{-1}$. These PPFD levels were chosen to reflect the natural variation in daylight and allowed for the development of light-response curves, similar to those used in CO_2[58] and volatile organic carbon (VOC)[59] flux modeling. Measurements were conducted on day 90 following *S. bebbiana* cutting establishment, when fully expanded foliage was present across all pots, using a single leaf per individual and five replicates per treatment, totaling 30 light-response measurements. Each leaf was allowed to acclimate for at least 10 min following a change in irradiance, and measurements were conducted between 9:00 and 13:00 local time. During these measurements, mean (±SE) leaf surface temperature was 26.08 ± 0.27 °C and relative humidity was 65.01 ± 2.29 %. To standardize for leaf developmental stage, the most recent fully-expanded leaf from each shoot was selected for measurements[60]. Across all measurements, the mean vapor pressure deficit (VPD) across all measurements was 1.61 kPa (range: 0.65–1.79 kPa). We also determined the light-response curve of stomatal conductance (mmol $H_2O \cdot m^{-2} \cdot s^{-1}$) in *S. bebbiana* (Supplementary Fig. 3). The collar diameter of each sampled individual (6.17 ± 0.31 mm) was also recorded. At the time of the experiment, the plants had an average height of 29.96 ± 2.25 cm.

Soil CH_4 and N_2O fluxes were measured in pots without willows with same set of treatments. PVC collars (10 cm in diameter, inserted to ~3 cm depth) were installed at least one day prior to soil flux measurements. A 10-cm soil respiration chamber (LI-COR 8100 A, LICOR Inc, Lincoln, Nebraska, USA) was coupled with the CH_4 and N_2O analyzers in closed-dynamic configuration to conduct simultaneous measurements of soil CH_4, N_2O, CO_2, and H_2O fluxes; each measurement lasted between 2–3 min.

Flux calculations

Leaf and soil CO_2, CH_4, H_2O, and N_2O concentration data obtained from both analyzers were first synchronized by date-time and converted to the same units (ppm) before calculating slopes. For slope calculation of each measurement, we excluded an initial (immediately after chamber closure) "dead-band" period– first ~10 s for leaves and 15 s for soil—to mitigate artefacts from chamber closure[61].

After removing the dead band, we applied a Pearson correlation coefficient (r)-based approach to identify the optimal time window for flux calculations. Specifically, we computed r between CO_2 concentration and time within a moving window (35 s for leaves, 60 s for soil). The time window yielding the highest r was subsequently used to calculate flux slopes (dc/dt) for all gases. CO_2 typically exhibits lower noise relative to CH_4 and N_2O, making it a reliable way to detect pressure disequilibria and select a window with well-mixed gas.

To calculate the slope (dC/dt) for CO_2, CH_4, H_2O, and N_2O fluxes, we utilized either linear or non-linear regression, following Halim et al.[62]. If the quadratic term in a polynomial fit was non-significant ($p > 0.05$), we used a linear fit, otherwise we choose a non-linear fit. Flux (F) was then computed using the following equation[63]:

$$F = \frac{10\ VP_o}{RS(T_o + 273.15)} \frac{dC}{dt} \quad (1)$$

where F is the flux of H_2O or water-corrected CO_2, CH_4, and N_2O. V is the total chamber headspace volume (cm^3), including the aboveground collar volume for soil. P_o is the initial gas pressure (kPa), R is the Universal Gas Constant (0.83144598 m^3 kPa k^{-1} mol^{-1}), S is the leaf/soil surface area (cm^2), T_o is the initial air temperature (°C), and dC/dt is the initial rate of change in the H_2O or water-corrected CO_2, CH_4, or N_2O mole fraction ($\mu mol \cdot mol^{-1} \cdot s^{-1}$). Throughout this paper, CO_2 fluxes are reported as $\mu mol \cdot mol^{-1} \cdot s^{-1}$, CH_4 fluxes as $nmol \cdot m^{-2} \cdot s^{-1}$, H_2O fluxes as $\mu mol \cdot m^{-2} \cdot s^{-1}$, and N_2O fluxes as $pmol \cdot m^{-2} \cdot s^{-1}$. All fluxes are expressed per unit area of the measured surface—soil fluxes per unit soil surface area, and foliar fluxes per unit leaf surface area.

For the non-linear patterns, we fitted the following empirical equation[64] to the data points of within the selected time window:

$$C'(t) = C'_x + \left(C'_0 - C'_x\right) e^{-a(t-t_0)} \quad (2)$$

where $C'(t)$ is the instantaneous H_2O, and water-corrected CO_2 or CH_4 or N_2O mole fraction, C'_o when the chamber just closed, C'_x is the asymptote parameter, a specifies the curvature of the fit (s^{-1}), and t_o is time (s) when the chamber closed. The parameters a, t_o, C'_x, and C'_o were estimated from the fitted nonlinear regression. Subsequently, using the following equation Eq. (3), which is derived from Eq. (2)(at t = t_o) was used to calculate the initial rate of change of the H_2O, and water-corrected CO_2, CH_4, or N_2O) mole fraction[63]:

$$\frac{dC}{dt} = a(C'_x - C'_0) \quad (3)$$

The resulting dC/dt value was then inserted into in Eq. (1) to obtain gas fluxes. Overall, using the above algorithm, 12% of CO_2 fluxes, 15% of CH_4 fluxes, 7% H_2O fluxes, and 11% N_2O fluxes required a non-linear fit, predominantly corresponding to high-flux measurements. We then averaged three replicate flux measurements per leaf and two replicate flux measurements per soil collar for further analyses.

Light curves and other non-linear model fitting

We evaluated various non-linear models for foliar CH_4, N_2O, CO_2, H_2O, and stomatal conductance light-response curves, drawing from established frameworks used to describe foliar CO_2 and isoprene fluxes. Ten candidate models—including the Hyperbola, Non-rectangular Hyperbola, Exponential, Rectangular Hyperbola, Modified Rectangular Hyperbola, Smith, Double Exponential, Polynomial, Generalized Poisson, and Sigmoid—were tested (Supplementary Tables 2 and 3). To assess model performance, we first examined the statistical significance of each parameter of the model and initial fit quality. We then further evaluate the models using multiple fit criteria such as the Akaike Information Criterion (AIC), Bayesian Information Criterion (BIC), ΔAIC, ΔBIC, and likelihood ratio tests (LRT) (Supplementary Table 4 and Supplementary Table 5). LRTs facilitated direct comparisons with a null model, limiting overfitting by ensuring that improved fits were statistically meaningful rather than artifacts of model complexity[65].

We applied a similar comprehensive comparison to identify optimal models relating foliar gas fluxes (CH_4 oxidation and N_2O emissions) to transpiration across different treatments. Eight candidate models—linear, cubic polynomial, exponential, power, Aguerre–Suarez–Viollaz (ASV), Aranovich–Donohue (AD), sigmoid, and Brunauer–Emmett–Teller (BET) isotherm[66]—were evaluated by residual standard error (RSE), Akaike Information Criterion (AIC), and Bayesian Information Criterion (BIC) (Supplementary Table 6). The model yielding the lowest AIC and BIC was selected for each treatment. Finally, to explore relationships between foliar

CH_4 and N_2O fluxes and soil variables such as CH_4 oxidation, total nitrogen content, specific leaf area (SLA), and N_2O emissions, we compared linear and four non-linear models to determine the best fit for these interactions (Supplementary Table 7).

For fitting the non-linear models, we employed the '*nlsLM*' function from the '*minipack.lm*' R-package, rather than the base '*nls*' function, to take advantage of the Levenberg-Marquardt algorithm[67]. This algorithm combines features of the Gauss-Newton and gradient descent methods, offering superior convergence properties, especially valuable for complex non-linear models. It also provides more robust initial parameter estimates, dynamically adjusting step sizes between gradient descent and Gauss-Newton steps, enhancing navigation through the parameter space. Additionally, *'nlsLM'* provides better convergence for intricate biological data by reducing the likelihood of becoming trapped in local minima. Parameters such as *'maxiter'*, *'ftol'*, *'ptol'*, and *'gtol'* provide additional fine-tuning options, further enhancing the stability of the optimization for complex biological processes like gas exchange.

Leaf and soil total N measurement

Leaf and soil samples were dried at 60 °C for 12 h and then finely ground (<0.5 mm). Prior to combustion, the ground samples were further dried for 30 min at 60 °C to remove any residual moisture. Each sample (20 g) was weighted before and after combustion to assess the loss of organic matter. Total nitrogen (N) content was determined using a LECO 628 Series CN analyzer (LECO Corporation, St. Joseph, MI, USA). During high-temperature combustion in an O_2-rich atmosphere, nitrogen was converted to nitrogen oxides (NO_x), which were subsequently quantified. Instrument calibration was performed using Elemental Drift Reference (EDR) standards, and quality control measures were employed to ensure reliable data.

Statistical analysis

All flux calculations and statistical analyses were conducted in R[68]. Linear mixed-effects models were fitted using the *'lme'* function[69] to evaluate the effects of light intensity and treatment on CH_4 and N_2O fluxes. Analysis of variance (ANOVA) was performed using the *'aov'* function from the *'stats'* package to determine significant treatment effects on fluxes. Where appropriate, Tukey's post-hoc tests (using *TukeyHSD*) were applied for pairwise comparisons.

Detection limits for the measured gas fluxes were estimated from the smallest statistically significant slopes in gas concentrations over time, observed across all foliar measurements: 0.01 $nmol \cdot m^{-2} \cdot s^{-1}$ for CH_4 and 0.007 $pmol \cdot m^{-2} \cdot s^{-1}$ for N_2O. To isolate leaf surface CH_4 oxidation and N_2O emission from transpiration and potential xylem-mediated transport, we employed a linear regression approach (*lm* in R). Flux rates at zero transpiration (0 $\mu mol \cdot m^{-2} \cdot s^{-1}$) were obtained by extrapolating from CH_4 or N_2O flux vs. H_2O flux regression models. We then evaluated whether these intercept-derived flux estimates differed significantly from zero via one-sample *t* tests, performing independent analyses for each treatment.

Data availability

The source data used to generate all graphs and charts presented in this study are publicly available via the Scholars Portal Dataverse repository at: https://doi.org/10.5683/SP3/GPT4XG[70].

Received: 31 January 2025; Accepted: 6 June 2025;
Published online: 21 June 2025

References

1. Nisbet, E. G. et al. Atmospheric methane and nitrous oxide: challenges alongthe path to Net Zero. *Philos. Trans. R. Soc. A: Math., Phys. Eng. Sci.* **379**, 20200457 (2021).
2. Pachauri, R. K. et al. *Climate Change 2014: Synthesis Report. Contribution of Working Groups I, II and III to the Fifth Assessment Report of the Intergovernmental Panel on Climate Change* (IPCC, Geneva, 2014).
3. Arias-Navarro, C. et al. Spatial variability of soil N_2O and CO_2 fluxes in different topographic positions in a tropical montane forest in Kenya. *J. Geophys. Res. Biogeosci.* **122**, 514–527 (2017).
4. Pangala, S. R. et al. Large emissions from floodplain trees close the Amazon methane budget. *Nature* **552**, 230–234 (2017).
5. Covey, K. R. & Megonigal, J. P. Methane production and emissions in trees and forests. *N. Phytologist* **222**, 35–51 (2019). vol.
6. Barba, J. et al. Methane emissions from tree stems: a new frontier in the global carbon cycle. *N. Phytologist* **222**, 18–28 (2019).
7. Karim, M. R., Halim, M. A. & Thomas, S. C. Foliar methane and nitrous oxide fluxes in tropical tree species. *Sci. Total Environ.* **954** (2024).
8. Qin, S. et al. Foliar N_2O emissions constitute a significant source to atmosphere. *Glob. Change Biol.* **30**, e17181 (2024).
9. Jones, H. G., editor. in *Plants and Microclimate: A Quantitative Approach to Environmental Plant Physiology* (ed. Jones, H. G.) 207–223 (Cambridge University Press, Cambridge, 2013). https://doi.org/10.1017/CBO9780511845727.009.
10. Coe, R. A. & Lin, H. Light-response curves in land plants. in *Photosynthesis: Methods and Protocols* (ed. Covshoff, S.) 83–94 (Springer New York, New York, NY, 2018). https://doi.org/10.1007/978-1-4939-7786-4_5.
11. Johnson, G. & Murchie, E. Gas exchange measurements for the determination of photosynthetic efficiency in ArabidopsislLeaves. in *Chloroplast Research in Arabidopsis: Methods and Protocols* Vol. II (ed. Jarvis, R. P.) 311–326 (Humana Press, Totowa, NJ, 2011). https://doi.org/10.1007/978-1-61779-237-3_17.
12. Herrmann, H. A., Schwartz, J. M. & Johnson, G. N. From empirical to theoretical models of light response curves - linking photosynthetic and metabolic acclimation. *Photosynthesis Res.* **145**, 5–14 (2020).
13. Timilsina, A. et al. Potential pathway of nitrous oxide formation in plants. *Front. Plant Sci.* **11** (2020).
14. Moisan, M. A., Lajoie, G., Constant, P., Martineau, C. & Maire, V. How tree traits modulate tree methane fluxes: A review. *Sci. Total Environ.* **940**, 173730 (2024).
15. Machacova, K. et al. Trees as net sinks for methane (CH_4) and nitrous oxide (N_2O) in the lowland tropical rain forest on volcanic Réunion Island. *N. Phytologist* **229**, 1983–1994 (2021).
16. Gauci, V. et al. Global atmospheric methane uptake by upland tree woody surfaces. *Nature* **631**, 796–800 (2024).
17. Gorgolewski, A. S., Caspersen, J. P., Vantellingen, J. & Thomas, S. C. Tree foliage is a methane sink in upland temperate forests. *Ecosystems* **26**, 174–186 (2023).
18. McGlynn, S. E. Energy metabolism during anaerobic methane oxidation in ANME archaea. *Microbes Environ.* **32**, 5–13 (2017).
19. Zhu, C. et al. Nitrogen and biochar addition affected plant traits and nitrous oxide emission from *Cinnamomum camphora*. *Front. Plant Sci.* **13** (2022).
20. Smart, D. R. & Bloom, A. J. Wheat leaves emit nitrous oxide during nitrate assimilation. *Proc. Natl Acad. Sci.* **98**, 7875–7878 (2001).
21. Pihlatie, M., Ambus, P., Rinne, J., Pilegaard, K. & Vesala, T. Plant-mediated nitrous oxide emissions from beech (*Fagus sylvatica*) leaves. *N. Phytol.* **168**, 93–98 (2005).
22. Nan, L. & Guanxiong, C. N_2O emission by plants and influence of fertilization. *Chin. J. Appl. Ecol.* **4**, 295–298 (1993).
23. Jeffery, S., Verheijen, F. G. A., Kammann, C. & Abalos, D. Biochar effects on methane emissions from soils: A meta-analysis. *Soil Biol. Biochem.* **101**, 251–258 (2016).
24. He, Y. et al. Biochar amendment boosts photosynthesis and biomass in C_3 but not C_4 plants: A global synthesis. *GCB Bioenergy* **12**, 605–617 (2020).
25. Rehman, M. Z. et al. Contrasting effects of biochar, compost and farm manure on alleviation of nickel toxicity in maize (*Zea mays* L.) in relation to plant growth, photosynthesis and metal uptake. *Ecotoxicol. Environ. Saf.* **133**, 218–225 (2016).

26. Sarma, B., Borkotoki, B., Narzari, R., Kataki, R. & Gogoi, N. Organic amendments: Effect on carbon mineralization and crop productivity in acidic soil. *J. Clean. Prod.* **152**, 157–166 (2017).
27. Karhu, K., Mattila, T., Bergström, I. & Regina, K. Biochar addition to agricultural soil increased CH_4 uptake and water holding capacity—results from a short-term pilot field study. *Agriculture, Ecosyst. Environ.* **140**, 309–313 (2011).
28. Cong, W., Meng, J. & Ying, S. C. Impact of soil properties on the soil methane flux response to biochar addition: a meta-analysis. *Environ. Sci.: Process. Impacts* **20**, 1202–1209 (2018).
29. Wang, S. et al. Photosynthesis, chlorophyll fluorescence, and yield of peanut in response to biochar application. *Front. Plant Sci.* **12** (2021).
30. Wang, Z. Y. et al. Effects of adding biochar on the properties and nitrogen bioavailability of an acidic soil. *Eur. J. Soil Sci.* **68**, 559–572 (2017).
31. Laird, D. A. et al. Impact of biochar amendments on the quality of a typical Midwestern agricultural soil. *Geoderma* **158**, 443–449 (2010).
32. Yamori, W., Kusumi, K., Iba, K. & Terashima, I. Increased stomatal conductance induces rapid changes to photosynthetic rate in response to naturally fluctuating light conditions in rice. *Plant, Cell Environ.* **43**, 1230–1240 (2020).
33. Raschke, K., Hanebuth, W. F. & Farquhar, G. D. Relationship between stomatal conductance and light intensity in leaves of *Zea mays* L., derived from experiments using the mesophyll as shade. *Planta* **139**, 73–77 (1978).
34. Sharkey, T. D. & Raschke, K. Separation and measurement of direct and indirect effects of light on stomata. *Plant Physiol.* **68**, 33–40 (1981).
35. Foyer, C. H. & Noctor, G. Photosynthetic nitrogen assimilation: Inter-pathway control and signaling. in *Photosynthetic Nitrogen Assimilation and Associated Carbon and Respiratory Metabolism* (eds. Foyer, C. H. & Noctor, G.) Vol. 12, 1–22 (Springer Netherlands, Dordrecht, 2002).
36. Abrol, Y. P., Sawhney, S. K. & Naik, M. S. Light and dark assimilation of nitrate in plants. *Plant Cell Environ.* **6**, 595–599 (1983).
37. Romdhane, L. et al. Wood biochar produces different rates of root growth and transpiration in two maize hybrids (*Zea mays* L.) under drought stress. *Arch. Agron. Soil Sci.* **65**, 846–866 (2019).
38. Doronina, N. V., Ivanova, E. G., Suzina, N. E. & Trotsenko, Yu. A. Methanotrophs and methylobacteria are found in woody plant tissues within the winter period. *Microbiology* **73**, 702–709 (2004).
39. Iguchi, H., Sato, I., Sakakibara, M., Yurimoto, H. & Sakai, Y. Distribution of methanotrophs in the phyllosphere. *Biosci., Biotechnol., Biochem.* **76**, 1580–1583 (2012).
40. Lieberman, R. L. & Rosenzweig, A. C. Biological methane oxidation: Regulation, biochemistry, and active site structure of particulate methane monooxygenase. *Crit. Rev. Biochem. Mol. Biol.* **39**, 147–164 (2004).
41. Sun, B., Zhao, H., LÜ, Y., Lu, F. & Wang, X. The effects of nitrogen fertilizer application on methane and nitrous oxide emission/uptake in Chinese croplands. *J. Integr. Agriculture* **15**, 440–450 (2016).
42. Steudler, P. A., Bowden, R. D., Melillo, J. M. & Aber, J. D. Influence of nitrogen fertilization on methane uptake in temperate forest soils. *Nature* **341**, 314–316 (1989).
43. Yang, N., Lü, F., He, P. & Shao, L. Response of methanotrophs and methane oxidation on ammonium application in landfill soils. *Appl. Microbiol. Biotechnol.* **92**, 1073–1082 (2011).
44. Putkinen, A. et al. New insight to the role of microbes in the methane exchange in trees: evidence from metagenomic sequencing. *N. Phytologist* **231**, 524–536 (2021).
45. Smirnoff, N., Winslow, M. D. & Stewart, G. R. Nitrate reductase acivity in leaves of barley (*Hordeum vulgare*) and durum wheat (*Triticum durum*) during field and rapidly applied water deficits. *J. Exp. Bot.* **36**, 1200–1208 (1985).
46. Guenther, A. B., Zimmerman, P. R., Harley, P. C., Monson, R. K. & Fall, R. Isoprene and monoterpene emission rate variability: Model evaluations and sensitivity analyses. *J. Geophys. Res.: Atmos.* **98**, 12609–12617 (1993).
47. Wang, X. et al. Effects of light on the emissions of biogenic isoprene and monoterpenes: A review. *Atmos. Pollut. Res.* **13**, 101397 (2022).
48. Zeng, J. et al. Temperature and light dependency of isoprene and monoterpene emissions from tropical and subtropical trees: Field observations in south China. *Appl. Geochem.* **155**, 105727 (2023).
49. Thomas, S. C., Gorgolewski, A. S. & Vantellingen, J. in *Forest Management for Climate Change Mitigation: Recent Innovations and Research Needs* (eds. Wang, Y. L Borja, M. E., Sun, Z. & Pereira, P.) 221–258 (Springer International Publishing, Cham, 2022). https://doi.org/10.1007/698_2022_937.
50. Saunois, M. et al. Global Methane Budget 2000–2020. *Earth Syst. Sci. Data Discuss.* **2024**, 1–147 (2024).
51. George, W. A. *Salix* (Salicaceae) distribution maps and a synopsis of their classification in north America, north of Mexico. *Harv. Pap. Bot.* **12**, 335–368 (2007).
52. Mosseler, A., Major, J. E. & Labrecque, M. Growth and survival of seven native willow species on highly disturbed coal mine sites in eastern Canada. *Can. J. Res.* **44**, 340–349 (2014).
53. Kayama, M., Kikuchi, S., Uemura, A. & Takahashi, M. Growth characteristics of seven willow species distributed in eastern Japan in response to compost application. *Forests* **14** (2023).
54. Yang, M. Increases in the methane uptake of upland forest soil in China could significantly contribute to climate change mitigation. *Forests* **13**, 1270 (2022).
55. Engineer, C. B. et al. CO_2 sensing and CO_2 regulation of stomatal conductance: advances and open questions. *Trends Plant Sci.* **21**, 16–30 (2016).
56. Ainsworth, E. A. & Rogers, A. The response of photosynthesis and stomatal conductance to rising [CO_2]: mechanisms and environmental interactions. *Plant Cell Environ.* **30**, 258–270 (2007).
57. Santiago, L. S. & Mulkey, S. S. A test of gas exchange measurements on excised canopy branches of ten tropical tree species. *Photosynthetica* **41**, 343–347 (2003).
58. Ögren, E. & Evans, J. R. Photosynthetic light-response curves. *Planta* **189**, 182–190 (1993).
59. Lerdau, M. & Gray, D. Ecology and evolution of light-dependent and light-independent phytogenic volatile organic carbon. *N. Phytologist* **157**, 199–211 (2003).
60. Thomas, S. C. & Bazzaz, F. A. Asymptotic height as a predictor of photosynthetic characteristics in Malaysian rain forest trees. *Ecology* **80**, 1607–1622 (1999).
61. Hoffmann, M. et al. A simple calculation algorithm to separate high-resolution CH_4 flux measurements into ebullition- and diffusion-derived components. *Atmos. Meas. Tech.* **10**, 109–118 (2017).
62. Halim, M. A., Bieser, J. M. H. & Thomas, S. C. Large, sustained soil CO_2 efflux but rapid recovery of CH_4 oxidation in post-harvest and post-fire stands in a mixedwood boreal forest. *Sci. Total Environ.* **930**, 172666 (2024).
63. LI-COR. *Using the LI-8100A Soil Gas Flux System and the LI-8150 Multiplexer*. 228 https://licor.app.boxenterprise.net/s/jtpq4vg358reu4c8r4id (2015).
64. Welles, J. M., Demetriades-Shah, T. H. & McDermitt, D. K. Considerations for measuring ground CO_2 effluxes with chambers. *Chem. Geol.* **177**, 3–13 (2001).
65. Araújo, M. C., Cysneiros, A. H. M. A. & Montenegro, L. C. Improved heteroskedasticity likelihood ratio tests in symmetric nonlinear regression models. *Stat. Pap.* **61**, 167–188 (2020).
66. Brião, G., de, V., da Silva, M. G. C., Vieira, M. G. A. & Chu, K. H. Correlation of type II adsorption isotherms of water contaminants using modified BET equations. *Colloid Interface Sci. Commun.* **46**, 100557 (2022).

67. Elzhov, T. V., Mullen, K. M., Spiess, A.-N. & Bolker, B. minpack.lm: R interface to the Levenberg–Marquardt nonlinear least-squares algorithm found in minpack, plus support for bounds. R package version 1.2-4, https://CRAN.Rproject.org/package=minpack.lm (2023).
68. R Core Team. *R: A Language and Environment for Statistical Computing* (R Foundation for Statistical Computing, 2024).
69. Pinheiro, J., Bates, D. & Team, R. C. Nlme: Linear and nonlinear mixed effects models. https://CRAN.R-project.org/package=nlme (2024).
70. Karim, M. R., Halim, M. A. & Thomas, S. C. Foliar fluxes of methane and nitrous oxide in *Salix bebbiana* respond to light and soil factors. Borealis, V1. https://doi.org/10.5683/SP3/GPT4XG (2025).

Acknowledgements

This research was supported by grants from the Natural Sciences and Engineering Research Council of Canada (NSERC). We thank Malaika Mitra, Melanie Sifton, and Imrul Kayes for their invaluable technical assistance and contributions to plant collection, soil analysis, and greenhouse preparation.

Author contributions

M.R.K. conceptualized the study, performed greenhouse preparation, data collection, and formal analysis. M.R.K. and M.A.H. conducted the investigation and contributed to software development. M.R.K. and S.C.T. designed the methodology. M.R.K., M.A.H. and S.C.T. performed data curation and analysis. M.A.H. contributed to writing—review and editing. S.C.T. provided supervision, funding acquisition, and conceptual oversight. M.R.K. wrote the original draft, with review and contributions from all authors.

Competing interests

The authors declare no competing interests.

Additional information

Supplementary information The online version contains supplementary material available at https://doi.org/10.1038/s43247-025-02453-4.

Correspondence and requests for materials should be addressed to Md Rezaul Karim.

Peer review information *Communications Earth & Environment* thanks Gavin McNicol and the other, anonymous, reviewer(s) for their contribution to the peer review of this work. Primary Handling Editor: Aliénor Lavergne. [A peer review file is available].